2D+Depth RF Localization via a Low-Cost Receiver

Tianyuan Du
University of Michigan
Ann Arbor, USA
alexdu@umich.edu

Yang-Hsi Su
University of Michigan
Ann Arbor, USA
devilsu@umich.edu

Alanson Sample
University of Michigan
Ann Arbor, USA
apsample@umich.edu

***Abstract*—The proliferation of mobile devices in consumer electronics, IoT, and healthcare sectors has sparked considerable interest in the field of wireless localization. While antenna array systems have demonstrated promise for wireless localization, they often entail high costs, intricate system designs, lengthy integration periods, and specialized packet formats. This study employs a 16-element L-shaped antenna array paired with a 2-channel 2MHz receiver, utilizing affordable and readily available components to localize incoming packets. The proposed approach calculates the 2D Angle of Arrival (AoA) of incoming signals using a custom Phase Difference Matching (PDM) algorithm. Additionally, a non-parallel wave depth estimator infers depth information of the signal source by learning phase difference trends. The result shows the system achieves median AoA accuracies of 2.53 degrees horizontally and 1.88 degrees vertically, with an average depth estimation error of 1.07 m. This approach demonstrates the potential for 3D wireless localization of commonly available RF devices, through an N-element 2D phased array paired with a cost-effective commodity receiver.**

***Index Terms*—AoA Estimation, Indoor Localization**

I. Introduction

Wireless localization is an emerging technology that powers various location-based services. These services include indoor navigation [1], asset tracking [2], healthcare [4], [5], augmented reality [6], [7], and smart home applications [3]. Over time, researchers have developed different techniques to locate wireless devices, relying on factors such as Received Signal Strength Indicator (RSSI) [11], [12], Angle of Arrival (AoA) [13]–[15], [19], and Time Difference of Arrival (TDoA) [9], [10] of the RF signal. Striking the right balance between localization accuracy, complexity, cost, and compatibility with existing devices is a goal for both academia and industry.

Among these techniques, AoA strikes a middle ground by offering better localization results than RSSI while demanding less hardware precision compared to TDoA. AoA-based systems calculate the angle of incoming RF signals using phased antenna arrays. By analyzing the phase differences of the RF signal received by separate antennas simultaneously, the RF signal's AoA can be determined. The accuracy of these results increases with the number of antennas in the array. However, challenges emerge when scaling up to large N-element arrays. Typically, each antenna requires a dedicated receiving channel, significantly inflating costs as the number of elements increases for synchronous receivers. To address this, RF switches are employed to connect multiple antennas sequentially to a single receiving channel [14], [18]. Nevertheless, as the receiver collects the RF signal from one antenna at a time, phase measurements from asynchronous samples can contain carrier frequency offsets (CFO) that affect AoA calculations. Existing solutions either require modifications to the packet structure or involve signal accumulation across multiple packets to provide a single AoA estimation [16]. Unfortunately, these approaches may not be compatible with existing consumer hardware or may slow down system response times. Additionally, achieving synchronization with the RF switch demands extra hardware and receiver modifications, adding to system costs and complexity. Lastly, attempts to perform 3D wireless device localization using AoA from a single receiver either has limitation in lower accuracy, or necessitates deploying multiple antenna arrays at various locations within the space, which can hinder system deployment and usability [15], [17].

This paper proposes a cost-effective solution utilizing affordable and readily available components to achieve precise 2D+ depth localization. The system comprises a 16-element phased antenna array with 2 RF mux, each switches through 8 antennas sequentially. The outputs of the two switches are connected to a 2-channel receiver operating at a 2MHz sampling rate, enabling the localization of existing, unmodified consumer devices such as smartphones. Notably, the RF switch timing is not synchronized with the RF receive chain, reducing overall costs and system complexity. After detecting, identifying the packet, and recovering the switch timing within the signal processing stage, the 2D Angle of Arrival (AoA) of the received packet is calculated with the Phase Differences Matching (PDM) algorithm. Additionally, depth information of the signal source is inferred using a non-parallel wave depth estimator, which learns the phase difference trends in the RF signals that deviate from the plane wave. The system attains a median 2D AoA accuracy of 2.53 horizontally and 1.88 degrees vertically, accompanied by an average depth estimation error of 1.07 m.

This paper provides the following contributions:

- A system for 2D AoA localization with two switched antenna arrays
- An phase difference matching algorithm for 2D AoA calculation
- An non-parallel wave depth estimator to infer depth from received phase

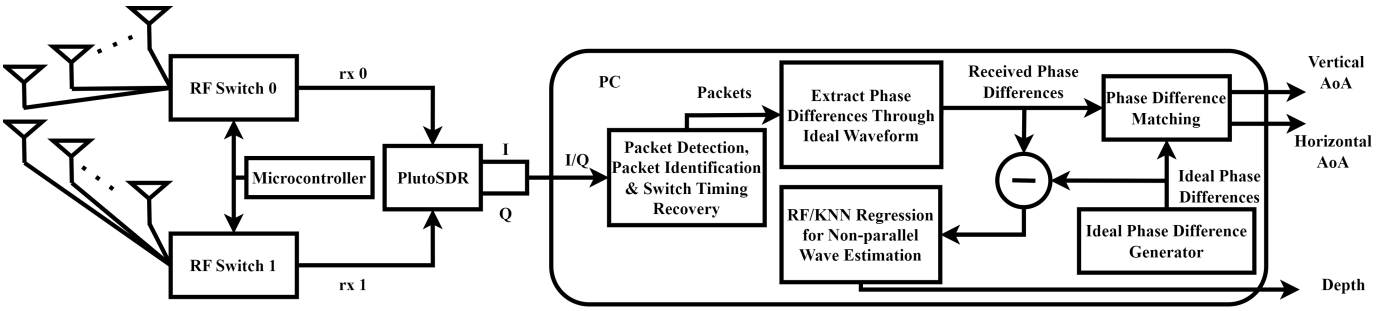

Fig. 1. The overall pipeline of the proposed system. The two RF muxs switch simultaneously controlled by a Teensy 4.0, and data are collected by a two-channel PlutoSDR, which are sent to a computer for processing. The signal processing pipeline includes packet detection and identification, switch timing recovery, phase difference extraction and ideal phase differences generation. Finally, Phase Difference Matching and non-parallel wave depth estimator are utilized to acquire AoA and depth, respectively.

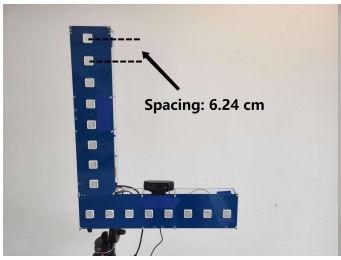

Fig. 2. Front View

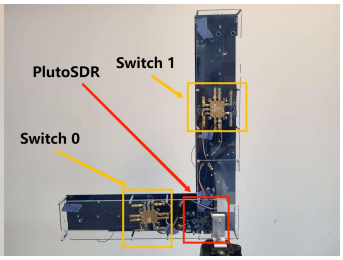

Fig. 3. Back View

Fig. 4. A picture of the L-shape antenna array. Each arm consists of 8 patch antennas. The spacing between the antennas is 6.24 cm, as half the wavelength of 2.402 GHz, the center frequency of BLE advertising channel 37. On the back view of the antenna arrays, the positions of the switches and PlutoSDR are marked out.

II. System Overview

This section outlines the system's hardware and signal processing flow, as shown in Fig. 1. At the core of the antenna array is a PlutoSDR, a budget-friendly 2-channel RF receiver operating at a 2MHz sampling rate. Each channel connects to an 8:1 RF multiplexer (mux) that sequentially routes signals from eight antennas. A microcontroller, a Teensy 4.0, is controlling the two RF switches simultaneously. This microcontroller operates independently from the receiver, following a predefined pattern to reduce extra hardware complexity and costs associated with synchronization. Importantly, previous research by Su et al. [18] has demonstrated the potential to recover switch timing during signal processing using this uncomplicated, low-cost hardware setup. The two 8-element arrays from the two receiving channels are combined into a single 16-element array, as depicted in Fig. 4. Data collected from the receiver is then transmitted to a PC for signal processing via a USB cable.

The software processing pipeline consists of multiple stages, as depicted in Fig. 1. Initially, the system detects and identifies valid packets from the incoming data stream. Subsequently, it recovers the microcontroller's switch timing by observing discontinuities in the received waveform. Once a packet is identified, an ideal packet waveform is generated to determine phase differences between antennas. The Phase Difference Matching (PDM) algorithm is then used to calculate the 2D Angle of Arrival (AoA) by comparing these phase differences with the ideal phase differences corresponding to each 2D angle. Finally, a depth estimation algorithm takes into account the non-ideal characteristics of incoming radio waves, which are not parallel, to estimate the depth of the signal source. Subsequent sections provide a more detailed explanation of each of these steps.

III. Methods and Algorithms

This section dives into the three essential signal processing blocks in Fig. 1, including the signal processing of packet detection, identification and switch timing recovery, Angle of Arrival (AoA) calculation with the Phase Differences Matching algorithm, and the non-parallel wave depth estimator for 3D localization.

A. Packet Detection, Identification, and Switching Timing Recovery

The BLE advertising packets transmitted from the target device are embedded in the received data stream. Since the antenna array is switching while receiving, the sudden change from one antenna to another introduces discontinuities in the waveform, causing bit errors when detecting and decoding packets. Existing approaches [18] showed that iBeacon type advertising packets can be detected and identified based on their distinct properties. Specifically, iBeacon advertising packets from different devices are different solely in their MAC address, UUID, and CRC. Packet detection is accomplished through the computation of correlation scores between the received phase derivative of a received waveform segment, and the phase derivative of an ideal iBeacon waveform, which is generated from Matlab's BLE Toolbox. When the correlation score surpasses a preset threshold, which is established empirically at 0.5, the presence of an iBeacon packet is confirmed. Subsequently, the packet would be decoded, and the UUID would be compared to a list of target UUID to identify whether the packet comes from any of the target devices.

After packets are detected and identified, received phases are matched to their corresponding antennas. In contrast to prior

research [14], the receive chain operates asynchronously with the RF switch, resulting in a lack of knowledge regarding the assignment of data segments in the received signal to specific antennas. To resolve this limitation, the system obtains switch timing by utilizing the discontinuity of the waveform. In this system, the microcontroller controls the RF switch in a pre-defined and continually repeating pattern. Switching the receiving antenna from one to another in the middle of receiving a packet creates jumps and spikes in the received magnitude and phase derivative waveform. The pre-defined switching pattern sets a unique sampling duration on each antenna, so when it is matched to the phase derivative segments in the received single-channel waveform, antenna assignment could be recovered. The packet detection, identification and antenna matching pipeline has proven to be effective in previous work [18].

B. Phase Difference Matching

This section presents the Phase Difference Matching (PDM) algorithm, a custom method that enables 2D AoA calculation by matching ideal phase differences with the received phase differences. This algorithm exemplifies cooperative use of vertically and horizontally placed antenna arrays to simultaneously determine the vertical and horizontal angles of arrival.

The PDM Algorithm comprises the preprocess phase and the runtime phase, where the preprocess phase consists of multiple distinct steps. Initially, ideal phase offsets are constructed for all possible antenna pairs, based on two AoAs: $AoA_{horizontal}$ in the x-z plane and $AoA_{vertical}$ in the y-z plane, both ranging from -90 degrees to 90 degrees, as presented in Fig. 5. This step accommodates all potential AoA scenarios and are executed before AoA measurements, which are in the runtime phase. Once $AoA_{horizontal}$ and $AoA_{vertical}$ are determined, the ideal phases of all 16 antennas are calculated, followed by the 16 phase differences between an arbitrarily determined null-antenna and every individual antenna. This involves converting $AoA_{horizontal}$ and $AoA_{vertical}$ into spherical coordinates ϕ and θ using the following mappings:

$$\theta = AoA_{horizontal} \tag{1}$$

$$\phi = \cot^{-1}\left(\sin\theta \tan AoA_{vertical}\right) \tag{2}$$

The positional relationship of θ, ϕ, $AoA_{horizontal}$ and $AoA_{vertical}$ are demonstrated in Fig. 5.

Subsequently, the distance differences between each antenna with the null antenna could be computed based on θ, ϕ and their coordinates. Suppose the null-antenna located at (x_0, y_0, z_0), the phase difference between the null-antenna and another antenna at position (x_p, y_p, z_p) could be calculated by

$$d = \sqrt{(x_0 - x_p)^2 + (y_0 - y_p)^2 + (z_0 - z_p)^2} \tag{3}$$

$$\Delta\hat{\psi}_p = 2\pi\left(\frac{d\cos\theta}{\lambda\cos\phi} - k\right) - \pi, p = 0, 1, 2, ...14, 15 \tag{4}$$

Where d implies the distance between the two antennas, $\Delta\hat{\psi}_p$ implies the estimated phase difference between antenna p and the null antenna, and λ implies wavelength of BLE signals. Notice that k implies aliasing effects, which happens when $d\cos\theta > \lambda\cos\phi$. To effectively remove aliasing, phase differences are shifted into the range of $-\pi$ to π. By iterating within the range in one-degree spacing ($-90°$ to $90°$) on both directions, the computation results in 181 by 181 vectors of 16 elements, each vector representing the ideal phase differences between an antenna and the null antenna. By this approach, the ideal phase differences cover a comprehensive range of spatial directions.

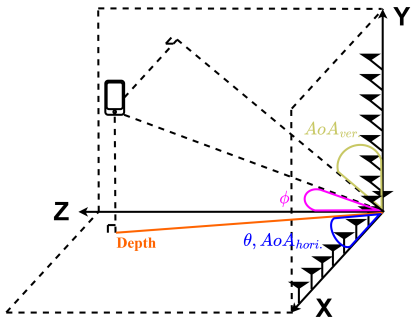

Fig. 5. Visual representation of the mapping from spherical angles to AoA described in Equation (1) and Equation (2). In practice, separately solving for the AoA on both antennas results in θ and the complementary angle of ϕ. To transform spherical angles to angles on the X-Z and Y-Z planes (horizontal and vertical AoA), previously mentioned equations are needed to construct the mapping.

During runtime, the processing operations are executed on a per-packet basis. Each antenna receives a segment of a packet, and the phase differences of antenna pairs are retrieved by comparing to an ideal waveform generated from the MATLAB BLE Toolbox. After iterating through a total of 16 antennas and getting each antenna's phase difference with the predetermined null-antenna that was initially selected during the preprocessing phase, identical steps of alias removal are performed. The runtime phase difference retrieval method is proven to be valid in prior work. [18]

The vector of obtained phase differences is compared with the 181 by 181 vectors of ideal phase differences. The objective is to pinpoint the 16-element ideal vector that most closely matches the obtained phase differences vector, defined by the lowest Mean Absolute Error (MAE) of their differences. Once this optimal vector is identified, the pair of its associated coordinates are extracted, which represents the estimated AoA(in degrees) in the horizontal and vertical directions respectively.

C. Non-parallel Wave Depth Estimator

Taking the system's localization capabilities one step further from the confines of 2D Angle of Arrival (AoA) measurement, 3D localization could be enabled with depth information. This research introduces non-parallel wave depth estimator, an algorithm that achieves depth estimation of target devices with only phase information.

In the context of 2D AoA estimation using phase difference of arrival, a fundamental assumption is that waves propagate

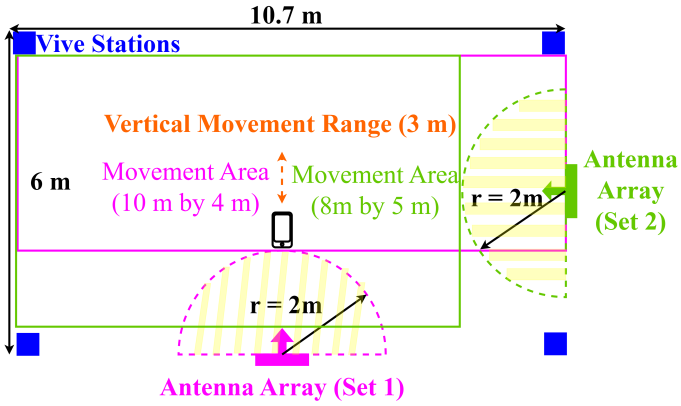

Fig. 6. A top-down view of the experiment setup. The designated area is 10.7 meters x 6 meters, with four vive base stations tracking a vive tracker for ground truth. A person holding a phone and a Vive tracker moves randomly within the purple area, and after the antenna position is changed, moves randomly within the green area.

as planar wavefronts. However, waves emitted from a single source are not planar in real-world indoor applications, and by analyzing the differences in the received signals compared to a planar wavefront assumption, it is possible to coarsely estimate the depth of the source. Analytical approaches assuming spherical wavefronts are challenging using real-world signals since the deviations are low in amplitude and can be corrupted by environmental factors such as noise and RF multipath. To overcome this challenge, correlation between non-parallelism in waves and object depth is investigated through machine learning on features extracted by associating each set of received phase differences with their post-filtering AoA values. The machine learning models of choice in this work are the K-Nearest-Neighbor(KNN) Regressor and Random Forest(RF) Regressor.

KNN regression is chosen for its ability to approximate the association between variables and continuous outcome, and to infer new data from these approximates as a non-parametric method. Random Forest Regression, on the other hand, excels at its ensemble learning nature, making it well-suited for handling noisy data with subtle features, which is the characteristic of Radio Frequency waveforms.

Upon each received vector of phase differences, identical preprocessing steps detailed in the preceding section are performed to generate ideal phase differences for the vertical and horizontal post-filtering AoA, as demonstrated in Equation (4). Subsequently, the inputs of machine learning pipelines are the differences between the received and the post-filtering estimated AoA's phase difference vectors, where the output is the estimated depth.

Considering the size of each dataset, KNN with K=500 and K=1000 are both examined, and the Random Forest Regressor contains 200 trees. Utilizing these machine learning models, depth estimation can be carried out using only phase information. Detailed experimental results are presented in the next section.

IV. Experiments and Evaluations

A. Experiment Setup

The area for experiments is an indoor office space with dimensions measuring 10.7 m by 6 m, and 3 m in height, denoted in Fig.6 and Fig.10. This area contains chairs, desks, and monitors that causes rich multipath, resembling real-world scenarios. Two experiments are designed and conducted with the purpose of assessing the system's effectiveness on measurement of 2D Angle of Arrival(AoA) and on depth estimation, respectively.

In both experimental scenarios, ground truth is retrieved using the Vive localization system with Vive Tracker 3.0, which was tracked by four base stations 2.0 positioned at the four corners of the experiment area, as demonstrated in Fig. 6. Both experiments employed the same iPhone 7 as the target localization device. This choice of equipment was motivated by smartphones' wide availability in the real world.

The antenna locations and participant movement range are shown in Fig. 6. During the experiment, a participant is invited to hold the Vive tracker closely to the iPhone and randomly move in the designated area marked in Fig. 6. In the first experiment, the participant moves in the purple area where the antenna array is put at the purple position, ranging 10 m by 4 m and height limit of 3 m. In the second experiment, the antenna array is put at the green location and the participant moves in the green area, ranging 8 m by 5 m and height limit of 3 m. For each random movement process, the participant is asked to walk and shift both the held objects up and down inside the designated test area for a continuous duration of 120 seconds, resulting in over 3000 to 3500 packets in one movement process. The random movements are done 5 times for the first experiment, and 5 times for the second experiment, consisting 16,352 and 14,218 data points respectively. Fig. 10 demonstrates the real experiment setup, where the antenna array and Vive stations are explicitly marked out.

In subsequent passages, data from the first experiment is denoted as Set 1, and data from the second experiment is denoted as Set 2. For Set 1, maximum depth reaches 7.2 meters, and for Set 2, maximum depth reaches 7.9 meters.

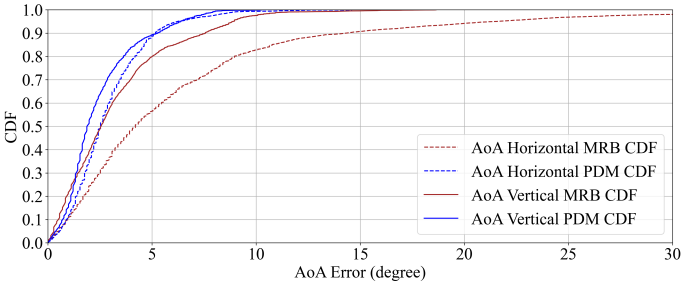

Fig. 7. CDF of 2D AoA results. For the Phase Difference Matching algorithm, 90% of the AoA errors are less than 6 degrees on both vertical and horizontal AoA, an improvement on MRB, which reaches 8 degrees and 12 degrees on 90%.

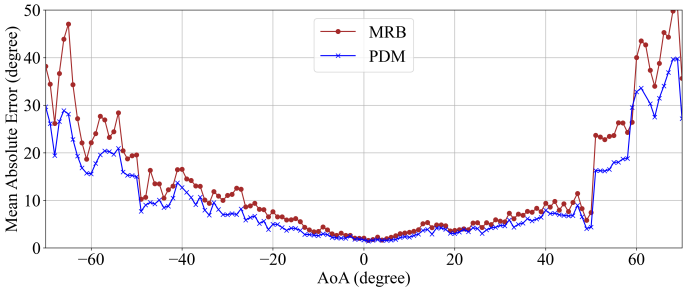

Fig. 8. Angle vs median error of horizontal AoA. From -30 to 30 degrees, PDM achieves error of less than 5 degrees, and within the range of -70 degrees to 70 degrees, PDM consistently outperforms MRB.

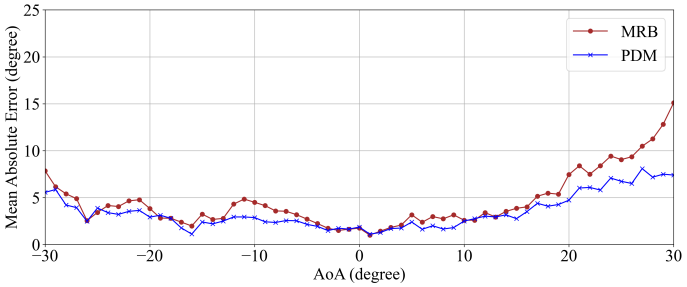

Fig. 9. Angle vs median error of vertical AoA. From -20 to 20 degrees, PDM achieves error of less than 5 degrees. It maintained its higher accuracy compared to MRB in the entire range of AoA, from -30 degrees to 30 degrees.

B. Performance of Two-Dimensional AoA

Set 1 data are used for evaluation of the effectiveness and accuracy of Phase Difference Matching (PDM) algorithm. Performance of both horizontal and vertical are plotted in blue in Fig. 8 and Fig. 9. To provide comparison, results from Multi-Resolution Beaming (MRB) proposed by Su et al. is plotted in red on each corresponding plots. [18] MRB is considered valid as it also performs AoA measurements on BLE signals with switched antenna array, and they utilized comparable hardware as this work proposes in the sense of cost and complexity. Results show that PDM has a lower error than MRB across the entire scope of measurement, ranging from -70 degrees to 70 degrees horizontally and -30 degrees to 30 degrees vertically. The evaluation used widely accepted matrices of Mean Absolute Error (MAE) and median errors.

The results of AoA measurements are presented in Fig . 8., Fig. 9 and Fig. 7. The proposed system demonstrated a commendable level of performance, yielding a median error of 2.53 degrees for horizontal AoA estimation and 1.88 degrees for vertical AoA estimation, where the median error for MRB yields 4.20 degrees for horizontal AoA and 2.55 degrees for vertical AoA, as demonstrated in Fig. 7. The figure also demonstrated the consistency of low error of PDM, as 90% of the errors are lower than 6 degrees. In the realm of two-dimensional (AoA) estimation, PDM surpassed MRB in both the horizontal and vertical orientations. Notably, PDM showcased a higher advantage particularly as the AOA measurements deviated further from 0 degrees, or the front direction. This underscores the effectiveness of PDM achieved through collaborative AoA measurements.

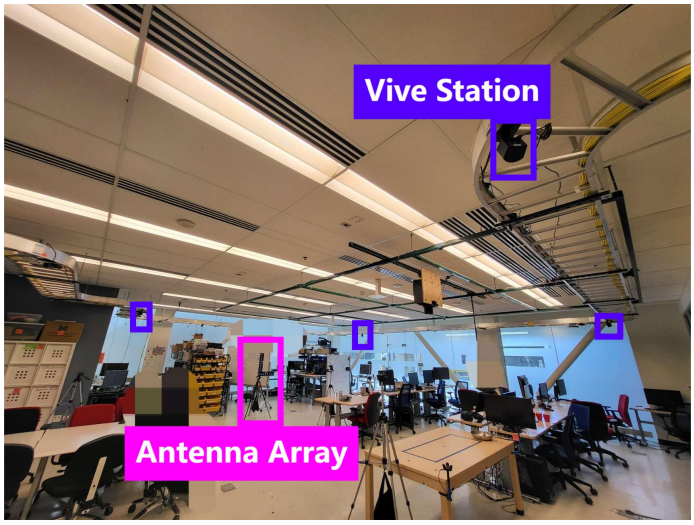

Fig. 10. The experiment environment as described in Fig. 6. The Vive base stations are marked in blue and the antenna array is marked in purple. The office space has obstacles including desks, chairs, monitors etc. that creates multipath.

C. Performance of Depth Estimation

Data from both Set 1 and Set 2 are used to assess the system's competence in performing depth estimation with a non-parallel wave depth estimator. Prior to applying machine learning on the collected data, both datasets go over a random shuffle. On each dataset, a 10 fold validation is performed. Additionally, as a comprehensive evaluation measure, performance of training on one dataset and testing on the other is also explored. Results are shown in 11, and median errors of all setup and model combinations are listed in table I.

Fig. 11 showcases the overall performance of the non-parallel wave depth estimator. Results show that training and testing on the same dataset or cross datasets provide similar results, suggesting that the machine learning approach is valid in capturing depth information. The proposed system

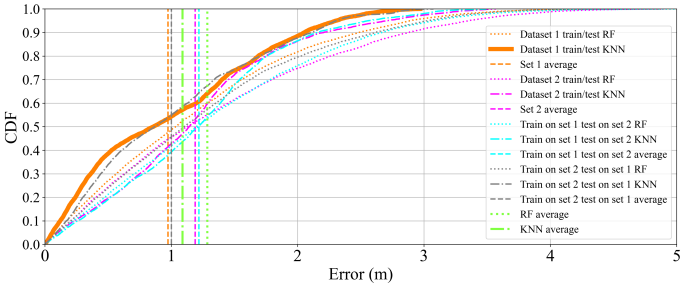

Fig. 11. CDF of depth error for non-parallel wave depth estimator. For the same dataset 10 fold validations, 90% of the errors are within 2.5 m. For cross dataset train-tests, 90% of the errors are within 3 m. Maximum depth of both datasets are over 7 m. The vertical lines show the average error in each train-test scenario and with each machine learning model. The heavy curve in orange demonstrates the most optimal performance.

TABLE I
DEPTH ESTIMATION

	Median Error of Depth	
	Random Forest	***KNN***
Set 1 10 Fold Vali.	1.04m	**0.86m**
Set 2 10 Fold Vali.	1.27m	**1.14m**
Train on Set 1 Test on Set 2	**1.20m**	1.21m
Train on Set 2 Test on Set 1	1.10m	**0.86m**

attains an average depth estimation error of 1.07 m on intra-dataset trained and tested data. The result is comparable with performance of prior research utilizing a 2D L-shape RF antenna array, which reported a median error of 1.06 m for 3D localization in a multipath-prone environment [15].

V. CONCLUSION

In conclusion, this paper presents an affordable and practical solution for achieving 2D+depth indoor localization using low-cost, readily available components. The proposed system leverages a 16-element L-shape phased antenna array with two RF multiplexers, enabling 2D Angle of Arrival (AoA) localization without the need for mux-receiver synchronization. Through a custom Phase Difference Matching (PDM) algorithm and a machine-learning based non-parallel wave depth estimator to infer depth, the system achieves median AoA accuracies of 2.53 degrees horizontally and 1.88 degrees vertically, with an average depth estimation error of 1.07 meter. Overall, the proposed system demonstrates effectiveness in 2D+depth localization with a single locator, which has the potential to enable a wide range of indoor localization applications.

REFERENCES

[1] H. Zou, B. Huang, X. Lu, H. Jiang and L. Xie, "Standardizing location fingerprints across heterogeneous mobile devices for indoor localization," 2016 IEEE Wireless Communications and Networking Conference, Doha, Qatar, 2016, pp. 1-6, doi: 10.1109/WCNC.2016.7564800.

[2] C. K. M. Lee, C. M. Ip, T. Park and S. Y. Chung, "A Bluetooth Location-based Indoor Positioning System for Asset Tracking in Warehouse," 2019 IEEE International Conference on Industrial Engineering and Engineering Management (IEEM), Macao, China, 2019, pp. 1408-1412, doi: 10.1109/IEEM44572.2019.8978639.

[3] Z. Turgut, G. Z. G. Aydin, and A. Sertbas, "Indoor localization techniques for smart building environment," Procedia computer science, vol. 83, pp. 1176–1181, 2016.

[4] Alberto Alvarez-Alvarez, Jose M. Alonso, and Gracian Trivino. 2013. Human activity recognition in indoor environments by means of fusing information extracted from intensity of WiFi signal and accelerations. Information Sciences 233 (2013), 162 – 182. https://doi.org/10.1016/j.ins.2013.01.029

[5] P. Barsocchi, S. Chessa, F. Furfari, and F. Potortì. 2013. Evaluating Ambient Assisted Living Solutions: The Localization Competition. IEEE Pervasive Computing 12, 4 (2013), 72–79.

[6] Luca Calderoni, Matteo Ferrara, Annalisa Franco, and Dario Maio. 2015. Indoor localization in a hospital environment using Random Forest classifiers. Expert Systems with Applications 42, 1 (2015), 125 – 134. https://doi.org/10.1016/j.eswa.2014.07.042

[7] Buti Al Delail, Luis Weruaga, M. Jamal Zemerly, and Jason W. P. Ng. 2013. Indoor localization and navigation using smartphones augmented reality and inertial tracking. In 2013 IEEE 20th International Conference on Electronics, Circuits, and Systems (ICECS). 929–932. https://doi.org/10.1109/ICECS.2013.6815564

[8] Steven J. Henderson and Steven Feiner. 2009. Evaluating the benefits of augmented reality for task localization in maintenance of an armored personnel carrier turret. In 2009 8th IEEE International Symposium on Mixed and Augmented Reality. 135–144. https://doi.org/10.1109/ISMAR.2009.5336486

[9] Manikanta Kotaru, Kiran Joshi, Dinesh Bharadia, and Sachin Katti. 2015. SpotFi: Decimeter Level Localization Using WiFi. In Proceedings of the 2015 ACM Conference on Special Interest Group on Data Communication (London, United Kingdom) (SIGCOMM '15). Association for Computing Machinery, New York, NY, USA, 269–282. https://doi.org/10.1145/2785956.2787487

[10] Ahmed Makki, Abubakr Siddig, Mohamed Saad, Joseph R Cavallaro, and Chris J Bleakley. 2015. Indoor localization using 802.11 time differences of arrival. IEEE Transactions on Instrumentation and Measurement 65, 3 (2015), 614–623.

[11] Yiran Peng, Wentao Fan, Xin Dong, and Xing Zhang. 2016. An iterative weighted KNN (IW-KNN) based indoor localization method in bluetooth low energy (BLE) environment. In 2016 Intl IEEE Conferences on Ubiquitous Intelligence and Computing, Advanced and Trusted Computing, Scalable Computing and Communications, Cloud & Big Data Computing, Internet of People, and Smart World Congress (UIC/ATC/ScalCom/CBDCom/IoP/SmartWorld). IEEE, 794–800.

[12] Kanyanee Phutcharoen, Monchai Chamchoy, and Pichaya Supanakoon. 2020. Accuracy Study of Indoor Positioning with Bluetooth Low Energy Beacons. In 2020 Joint International Conference on Digital Arts, Media and Technology with ECTI Northern Section Conference on Electrical, Electronics, Computer and Telecommunications Engineering (ECTI DAMT & NCON). IEEE, 24–27

[13] X. Jiang and S. Wang, "Cooperative Localization in Wireless Sensor Networks with AOA Ranging Measurements," 2020 IEEE Wireless Communications and Networking Conference (WCNC), Seoul, Korea (South), 2020, pp. 1-6, doi: 10.1109/WCNC45663.2020.9120806.

[14] Zhihao Gu, Taiwei He, Junwei Yin, Yuedong Xu, and Jun Wu. 2021. TyrLoc: a low-cost multi-technology MIMO localization system with a single RF chain. In Proceedings of the 19th Annual International Conference on Mobile Systems, Applications, and Services. 228–240.

[15] L. Zhang and H. Wang, "3D-WiFi: 3D Localization With Commodity WiFi," in IEEE Sensors Journal, vol. 19, no. 13, pp. 5141-5152, 1 July1, 2019, doi: 10.1109/JSEN.2019.2900511.

[16] Marco Cominelli, Paul Patras, and Francesco Gringoli. 2019. Dead on Arrival: An Empirical Study of The Bluetooth 5.1 Positioning System. In Proceedings of the 13th International Workshop on Wireless Network Testbeds, Experimental Evaluation amp; Characterization (Los Cabos, Mexico) (WiNTECH '19). Association for Computing Machinery, New York, NY, USA, 13–20. https://doi.org/10.1145/3349623.3355475

[17] E. Sippel, M. Lipka, J. Geiß, M. Hehn and M. Vossiek, "In-Situ Calibration of Antenna Arrays Within Wireless Locating Systems," in IEEE Transactions on Antennas and Propagation, vol. 68, no. 4, pp. 2832-2841, April 2020, doi: 10.1109/TAP.2019.2955147.

[18] Yang-Hsi Su, Chouchang Jack Yang, Euiseok Hwang, and Alanson P. Sample. 2023. Single Packet, Single Channel, Switched Antenna Array for RF Localization. Proc. ACM Interact. Mob. Wearable Ubiquitous Technol. 7, 2, Article 76 (June 2023), 25 pages. https://doi.org/10.1145/3596263

[19] P. Sambu and M. Won, "An Experimental Study on Direction Finding of Bluetooth 5.1: Indoor vs Outdoor," 2022 IEEE Wireless Communications and Networking Conference (WCNC), Austin, TX, USA, 2022, pp. 1934-1939, doi: 10.1109/WCNC51071.2022.9771930.